Fluid Phase Equilibria 498 (2019) 151–159

Contents lists available at ScienceDirect

Fluid Phase Equilibria

journal homepage: www.elsevier.com/locate/fluid

Calculation of viscosities of branched alkanes from 0.1 to 1000 MPa by molecular dynamics methods using COMPASS force field

Nikolay D. Kondratyuk [a, b, c, *], Vasily V. Pisarev [b, c]

[a] Moscow Institute of Physics and Technology (National Research University), Institutskiy Pereulok, 9, Dolgoprudny, 141701, Russia
[b] Joint Institute for High Temperatures of RAS, Izhorskaya st. 13 Bd.2, Moscow, 125412, Russia
[c] National Research University Higher School of Economics, Myasnitskaya ulitsa, 20, Moscow, 101000, Russia

ARTICLE INFO

Article history:
Received 28 February 2019
Received in revised form
25 June 2019
Accepted 26 June 2019
Available online 29 June 2019

Keywords:
Molecular dynamics
Shear viscosity
Green-Kubo method
Branched alkanes

ABSTRACT

Shear viscosity is one of the key subjects of molecular modeling studies since this quality is used in the development of lubricants. In this paper, we use molecular dynamics methods to predict viscosity dependence on pressure up to 1000 MPa for 2,2,4-trimethylhexane. The COMPASS class II force field is used to determine atomic interactions in the model. The shear viscosity is calculated using Green-Kubo and Müller-Plathe methods. To achieve the convergence of the Green-Kubo integral, the time decomposition method is used. The approach is validated by 2,2,4-trimethylpentane for which experimental data are available. The calculated 2,2,4-trimethylhexane viscosity coefficient dependence is fit by Tait-like equation and does not show super-Arrhenius behavior. The Tait fit matches the experiment produced by Scott Bair for the pressures up to 500 MPa within the accuracy of the methods.

1. Introduction

Modern industry is strongly interested in studying the properties of liquid hydrocarbons since they are components of the lubricants, insulation and fuel liquids. The properties that play a major role in the process of elasto-hydrodynamic lubrication (EHL) are the shear viscosity dependence on pressure and the pressure viscosity coefficient [1]. The classical film thickness formulas require the latter property, but it is not always clear how to define it [2]. The viscosity dependence on pressure determines the shape of friction curve (friction coefficient vs. sliding speed) of oil films [3]. However, such dependencies are often not measured experimentally in the EHL analysis, and the demand for such kind of data is growing in recent years.

The molecular dynamics (MD) techniques proved useful for the estimation of such properties [4,5]. There are two approaches for the calculation of the shear viscosity coefficient in the MD simulations. The first one is a Green-Kubo (G-K) relation [6] in which viscosity can be found as a time integral of shear stress autocorrelation function (SACF). SACF is calculated from equilibrium MD simulation. The second family of methods are non-equilibrium MD (NEMD) simulations in which viscosity coefficient is found from the ratio of the shear stress to the velocity gradient [7–9]. There are various works on systems where G-K integral converges without problems [10–13]. Maginn and coauthours in 2015 proposed a technique to circumvent the convergence problems in the G-K method for highly viscous liquids [14]. It is called time decomposition method and has been successfully applied for ionic liquids [15] and hydrocarbons [16]. The accurate error estimation of the G-K method for Lennard-Jones liquid has been done by Kim and coauthors in 2018 [17].

The problems with convergence in G-K for the systems of complex molecules can be avoided by using NEMD methods instead for viscosity calculations. The comparison of those methods is done by Hess for the cases of Lennard-Jones liquid and water [18]. NEMD methods have been used for lubricants viscosity calculations [19]. However, the shear viscosity of the high viscous systems depend on the shear rate and should be extrapolated to the zero shear rate. Evans and Cummings make such extrapolations for liquid rubidium, sodium and water in Ref. [20]. Moore and Cummings calculate zero shear rate viscosity of the *n*-alkane liquids in Ref. [21]. Several works demonstrate that the Newtonian regime is achievable without any extrapolation even in the complex cases for the hydrocarbons [22–27]. The recent work made by Jadhao in 2017 [28] shows a technique how to extrapolate the NEMD results on viscosity calculations of squalane to the equilibrium Newtonian

* Corresponding author. Moscow Institute of Physics and Technology (National Research University), Institutskiy Pereulok, 9, Dolgoprudny, 141701, Russia.
E-mail address: kondratyuk@phystech.edu (N.D. Kondratyuk).

https://doi.org/10.1016/j.fluid.2019.06.023
0378-3812/

viscosity that is measured in the experiment.

There are series of works on MD simulations of viscous properties of hydrocarbons in the past two decades. Allen in 1997 [29] made an attempt to predict the 2,2,4-trimethylpentane shear viscosity at 0.1 MPa from MD simulations with OPLS-AA [30] and OPLS-UA [31] force-fields using NEMD. The OPLS-AA potential value lies very close to the experimental data at 0.1 MPa. Lahtela and coauthors have studied how branching influences the viscous properties of eicosane isomers using NEMD [32], and they show that a branch at carbon 2 in chain significantly increases viscosity. The calculations of kinematic viscosity of three $C_{30}H_{62}$ isomers which are lubricant basestocks are done in Ref. [21]. The dependence of the viscosity coefficient on pressure is studied using NEMD for the branched hydrocarbons at pressures up to 400 MPa in Ref. [22], for 9-octylheptadecane at pressures up to 1 GPa in Ref. [24] and for squalane at 0.3 GPa in Ref. [25]. The temperature dependence of viscosity for 9-octylheptadecane is calculated in Ref. [23]. The detailed comparison of the classical force fields is made in Ref. [19] in terms of prediction of lubricants viscosity. The pressure dependence of viscosity for squalane is predicted in the work by Jadhao and Robbins [28] which references the extensive experimental work [33]. However, there are no simulations in the region of the super-Arrhenius pressure dependence of viscosity which is important to friction [3].

The aim of the current work is a prediction of viscous properties for 2,2,4-trimethylhexane for which no experimental data is available during the Industrial Fluid Properties Simulation Challenge. This compound is a candidate that has the super-Arrhenius viscosity dependence. We find a homologous molecule 2,2,4-trimethylpentane for which a lot of experimental studies are done. Its chain is only one carbon atom shorter, so we expect it to have a similar $\eta(P)$ dependence. The dependence of 2,2,4-trimethylpentane viscosity on pressure is studied experimentally by Dymond in 1985 [34] (for pressures up to 500 MPa) and Padua in 1996 [35] (for pressures up to 100 MPa). The viscosity as a function of pressure is fitted by a Tait-like equation [36] in Dymond's paper [34]. This fitting function requires the value of η at 0.1 MPa.

Here, we use molecular dynamics methods to compute the shear viscosity coefficients for 2,2,4-trimethylpentane and 2,2,4-trimethylhexane liquids. The rest of the paper is arranged as follows. In Section 2, details about force field, molecular simulation technique and system equilibration are presented. Section 3 contains the information about the methods used for the shear viscosity calculations. The calculated viscosity dependencies on pressure for 2,2,4-trimethylpentane and 2,2,4-trimethylhexane and their comparison with the experimental data in the case of 2,2,4-trimethylpentane are discussed in Section 4.

2. Modeling and simulation techniques

2.1. Force field

The choice of the force field determines the properties that can be obtained from simulations. For the theoretical studies, authors usually use simple models such as point particle models [37–41], coarse-grained [42] and united atom models [43] that give qualitative results to verify or expand theory. If ones need accurate estimation of properties, more complex models should be used [44–52].

In the previous work [53], we studied how different class I force fields reproduce the equation of state and diffusivity of non-branched n-triacontane $C_{30}H_{62}$. The potential energy of the molecular liquid can be modeled as follows:

$$E = E_{bond} + E_{angle} + E_{dihedral} + E_{improper} + E_{VdW} + E_{Coul}, \quad (1)$$

where bond, angle, dihedral and improper are intramolecular atomic interactions, Van der Waals and Coulomb forces act between atoms inside one molecule and between atoms of different molecules.

Allen and Rowley in 1997 compare OPLS-AA and OPLS-UA in terms of the viscosity prediction of different hydrocarbons at 0.1 MPa. The value of η for 2,2,4-trimethylpentane lies very close to the experimental data, but the pressure dependence is not considered. In the recent study [19], Ewen compares different united- and all-atom force fields for MD simulations of lubricants (n-hexadecane), 3 pressures up to 200 MPa are considered.

The hydrocarbons equations of state are strongly influenced by the intermolecular interactions (see, e.g., Ref. [54]). O'Connor shows that Lennard-Jones 6–12 form for nonbonded interactions fails to reproduce properties of carbon systems under extreme conditions. The problems are caused by the strong repulsion term presented by $1/r^{12}$. We think that the force fields described above would fail to reproduce the viscosity at high pressures relying on the O'Connor's [55] work.

Therefore, we decide to try COMPASS (condensed-phase optimized molecular potentials for atomistic simulation studies) class II force field [56] for the prediction of viscosity coefficient as a function of pressure. In the class II force fields, the bonds and angles are described by the non-harmonic functions, and all the intramolecular interactions exchange energy via cross terms. The Van der Waals nonbonded interactions in COMPASS are presented via 6–9 form which, we expect, gives more trustworthy results at the pressures of the order of 1 GPa. All the interaction parameters [56] are given on the LAMMPS user forum [57]. The molecular topology and force field parameters are given in Supporting Information.

2.2. Details of molecular dynamics simulations

All the calculations are performed for the equilibrated systems of the 1000 molecules. Since the viscosity does not depend on the size effects [16,58] that take place in the diffusivity case [16,53,59,60], only this box size is considered. Non-bonded 1–4 interactions are not scaled. The cut off radius for non-bonded forces is 12 Å, long-range Coulomb interactions are calculated using the particle-particle particle-mesh method [61] with the desired relative error in forces 10^{-5}. The tail corrections for the pressure are also applied. The equations of motion are integrated using rRESPA algorithm [62] with a timestep of 1 fs for Lennard-Jones and Coulomb interactions. The bonds and angles are treated with 0.125 fs, the dihedrals and impropers with 0.5 fs timestep. The simulations are performed in periodic boundary conditions (PBC) using the LAMMPS package [63] with the use of GPU package [64–66]. Such simulations require a lot of computational resources, so the optimization of the hardware is considered [67–70].

2.3. System equilibration

The equilibration procedure is done in the following way. The molecular topology and force field data are generated using *msi2lmp* tool in LAMMPS. The initial configuration is 1000 randomly oriented molecules at the density 0.7 g/cm^3. The viscosity is insensitive to the system size [16,17], unlike the self-diffusion coefficient which requires size corrections to be calculated precisely [59]. At the first stage, the energy minimization is performed. After that, the atoms gain random velocities with the average corresponding to the temperature 293 K, and the system relaxes in Langevin thermostat for 50 ps. After this step, the thermostat is

switched off and equations of motion are integrated using *nve/limit* command in LAMMPS, which restricts the maximal displacements of atoms in one timestep, preventing ejection of atoms due to possible overlapping of molecules during relaxation. The third stage is the relaxation in the isothermal-isobaric ensemble (NPT) for 2 ns with the required pressure. The average density during this stage is chosen as the equilibrium density for the given pressure. The fourth stage is compression to the equilibrium density for 200 ps. The last stage is relaxation in the canonical ensemble (NVT) for 2 ns. The total linear momentum of the system is zeroed at the end of the relaxation process because any drift of the center of mass (that can be created during the relaxation process) impairs the accuracy of viscosity calculation. The example of unit cell is presented on Fig. 1.

The viscosity calculations for 2,2,4-trimethylpentane and 2,2,4-trimethylhexane are performed in the microcanonical ensemble (NVE) for the obtained densities that are shown on Fig. 2a and b. The 2,2,4-trimethylpentane liquid is used for the verification of the used model. Fig. 2a shows density data from the experimental works [34,35] (filled blue and black circles correspondingly). One can see that both experimental $P-\rho$ curves are in close agreement. The reported experimental errors are less than the size of the points. The $\rho(P)$ dependence can be fitted by the Tait-like equation [36] which is shown to give accurate approximations for gases, liquids and solids:

$$(\rho-\rho_0)/\rho = C\cdot\log_{10}[(B+P)/(B+P_0)], \quad (2)$$

where ρ_0 is a density at P_0, ρ is a current density at pressure P, C and B are the fitting constants. The usual choice of P_0 is 1 bar = 0.1 MPa.

The fits represent the results with a good accuracy. The calculated densities from the NPT simulations (red open circles) are slightly overestimated, with the deviation from the experimental data (blue filled circles) [34] growing with the increase of pressure and reaching 2% (Fig. 2a) at 500 MPa. This effect has an influence on the viscosity prediction and is discussed in Section 4.

The fitting constants for 2,2,4-trimethylpentane and 2,2,4-trimethylhexane are presented in Table 1. The applicability of Eq. (2) to both experimental and MD data reflects the fact that the MD model predicts the compression of the liquid qualitatively, but the values of the density can be overestimated. Therefore, the correction for the viscosity should be applied based on the estimations for 2,2,4-trimethylpentane.

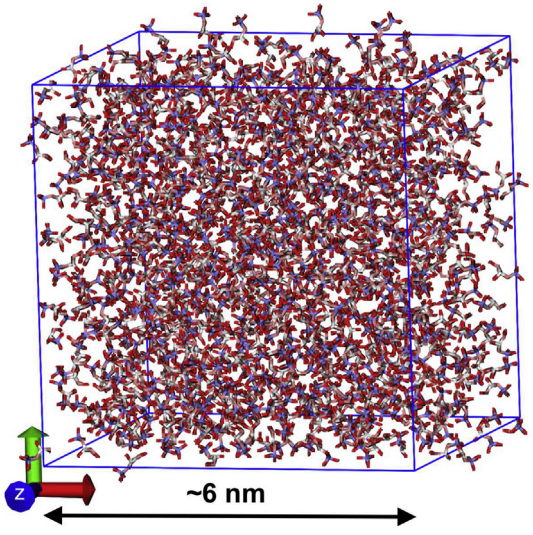

Fig. 1. The snapshot of the simulation cell of 2,2,4-trimethylhexane at $T = 293$ K and $P = 0.1$ MPa. The number of molecules is 1000. The hydrogen atoms are not shown. The carbon atoms are colored by the value of charge.

3. Shear viscosity calculations

3.1. Müller-Plathe method

The viscosities of liquids and fluids can be calculated by the reverse non-equilibrium molecular dynamics (RNEMD) approach [9]. This approach imposes momentum transfer in the simulation cell. As a response, a velocity gradient is established. The ratio of the momentum flux to the velocity gradient gives the shear viscosity:

$$\eta = \frac{j_z(p_x)}{\partial v_x/\partial z} \quad (3)$$

where $j_z(p_x)$ is the flux of the x-component of momentum in the z direction.

The flow in the liquid is created via the *fix viscosity* command in LAMMPS. The cell is divided into 50 bins in Z direction, and the average velocity of group of atoms in each layer is calculated. The MD trajectory lengths that are used to produce the velocity profiles are 3 ns. The first 50 ps are neglected due to the flow establishment. For the example, the velocity profiles in 2,2,4-trimethylhexane at 150, 250, 400 and 500 MPa are shown on Fig. 3a. The x-axis corresponds to the current location in the z-direction divided by the box length. The viscosity can be found by dividing the momentum flux by the velocity gradient. The results are presented on Fig. 3b. The filled circles of the same color show the values of viscosity at the various shear rates. The color reflects the pressure. The more red points correspond to the higher pressures. Dotted lines are connecting the data points to guide the eye.

The problem of this method is that the shear viscosity coefficient depends on the shear rate $\dot{\gamma} = \partial v_x/\partial z$ (Fig. 3b). We expect that the experiment is made for $\dot{\gamma}$ below 10^5 s^{-1} where liquid is Newtonian. The problem is that such shear rates are too low for direct MD simulations. Therefore, we operate with high shear rates above 10^7 s^{-1}. There are two different types of liquids which are determined by their behavior at the high shear rates. The first one, called shear thickening liquids, have the viscosity starts growing with the strain rate after the Newtonian region at low $\dot{\gamma}$ where η is almost constant. The second one, called shear thinning liquids, have the decreasing viscosity dependence on the shear rate. Carreau proposed a generalized equation on how it should depend on the $\dot{\gamma}$:

$$\eta(\dot{\gamma}) = \eta_{inf} + \left(\eta_0 - \eta_{inf}\right)\left(1 + ((\lambda\dot{\gamma})^2\right)^{(n-1)/2}, \quad (4)$$

where η_0 and η_{inf} are viscosities at zero and infinite shear rate, respectively, η is a viscosity at shear rate $\dot{\gamma}$, λ is a relaxation time and n is a power that depends on the type of the liquid.

The solution is to calculate the shear viscosity as a function of the shear rate and approximate this data to the zero shear rate. However, in highly viscous liquids, it becomes difficult to establish weak flows, and very long MD trajectories required. The available shear rates for such systems produce the values of viscosity that are beyond the Newtonian regime. The extrapolation technique is proposed by Jadhao and Robins in 2017 [28] with the help of Eyring model to extrapolate NEMD viscosity to the Newtonian region for the glass-former squalene $C_{30}H_{62}$.

In the case of 2,2,4-trimethylhexane, the same problems appear with the increase of pressure. At the higher pressures (Fig. 3b), the Newtonian regime becomes unattainable by RNEMD. The extrapolation technique [28] requires the same amount of computational resources as equilibrium Green-Kubo calculations described in the

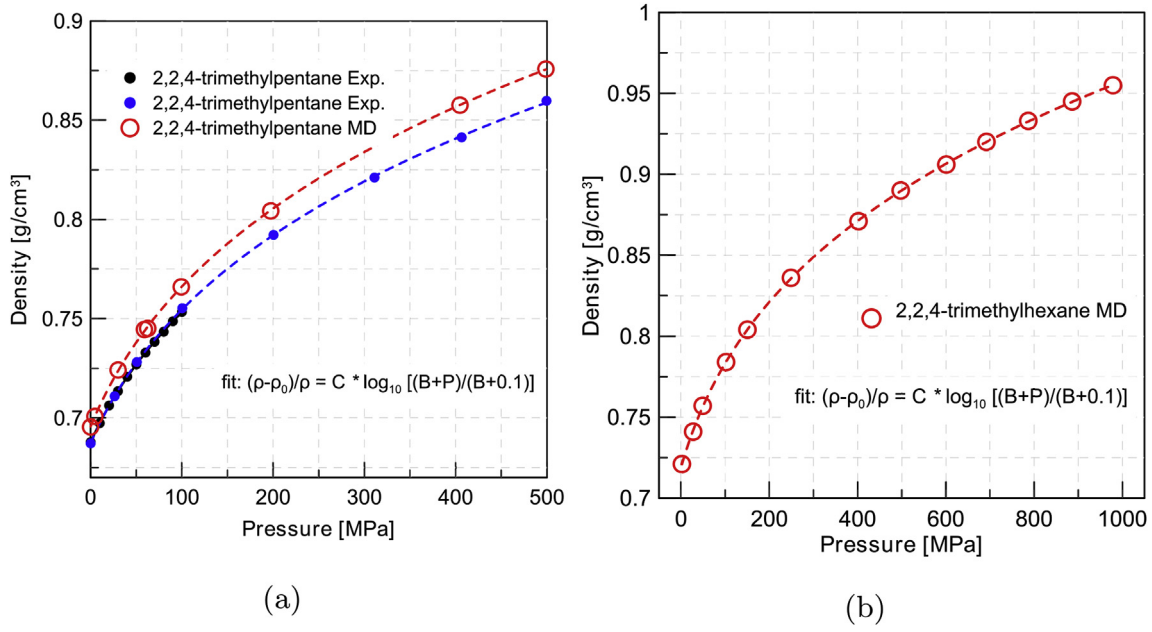

Fig. 2. The densities dependencies on pressure for 2,2,4-trimethylpentane (a) and 2,2,4-trimethylhexane (b) liquids. Red open circles are NPT simulations results. Blue and black filled circles are the experimental data [35,36].

Table 1
The fit parameters C and B for Eq. (2) for the experimental and simulation data for 2,2,4-trimethylpentane and 2,2,4-trimethylhexane.

Compound	Method	C	B [MPa]
2,2,4-trimethylpentane	Exp.	0.2	56
	MD	0.2	55
2,2,4-trimethylhexane	MD	0.2	67

next section. Thus, we decide to use Green-Kubo relation instead of RNEMD because it allows to calculate the viscosity coefficient at the zero shear stress directly. The comparison of the values obtained by two different methods makes the results self-consistent.

3.2. Green-Kubo method

The Green–Kubo formula for the shear viscosity $\eta_{\alpha\beta}$ in $\alpha\beta$-plane is [6]:

$$\eta_{\alpha\beta} = \lim_{t' \to \infty} \frac{V}{k_B T} \int_0^{t'} C_\sigma(t) dt, \tag{5}$$

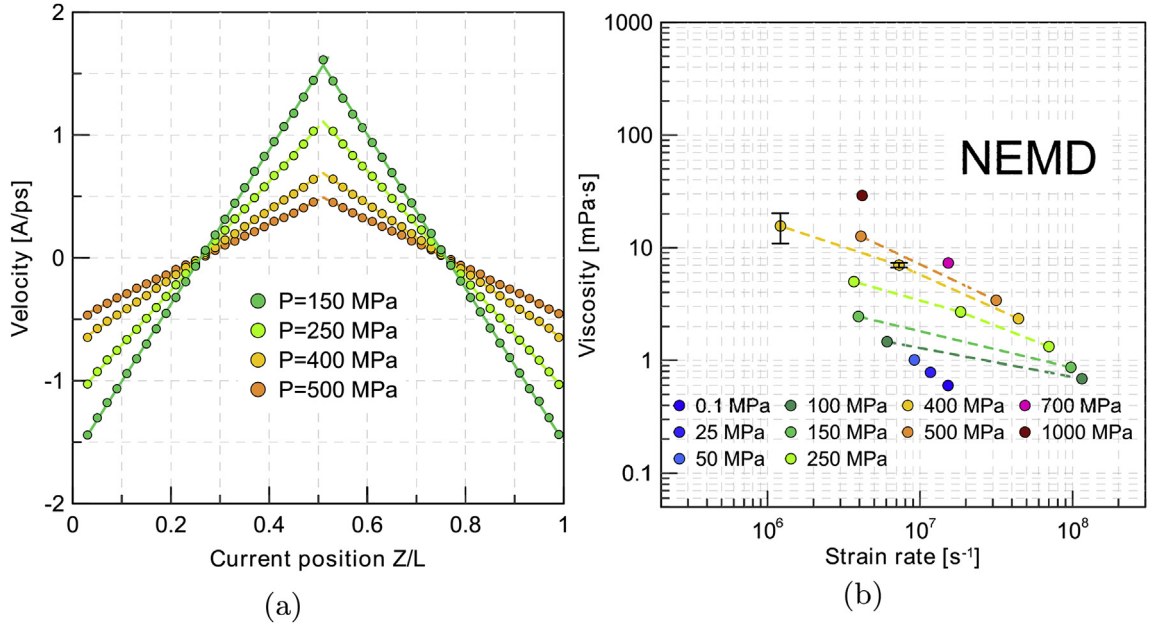

Fig. 3. The averaged velocity profiles in liquid 2,2,4-trimethylhexane at different pressures (a) and the shear viscosities η at the different pressures as functions of shear rate $\dot{\gamma}$ (b). The errors for NEMD values are calculated during the fitting procedure (described in Supporting Information).

$$C_\sigma(t) = \langle \sigma_{\alpha\beta}(0)\sigma_{\alpha\beta}(t)\rangle, \quad (6)$$

where $C_\sigma(t)$ is an autocorrelation function, $\sigma_{\alpha\beta}$ are off-diagonal components of the stress tensor, V and T are system volume and temperature, and k_B is Boltzmann's constant. In practice, the integral in (5) is typically calculated up to some time t' when C_σ decays to zero to the accuracy of numerical simulation. $\langle \ldots \rangle$ in (6) is an average over the canonical ensemble. The shear viscosity η is found as an average of the η_{xy}, η_{xz} and η_{yz}.

The stress tensor $\sigma_{\alpha\beta}$ is calculated from the following equation:

$$\sigma_{\alpha\beta}V = \sum_{i=1}^{N} m_i v_{i_\alpha} v_{i_\beta} + \sum_{i=1}^{N} r_{i_\alpha} f_{i_\beta}, \quad (7)$$

where N is a number of atoms, r_{i_α} and v_{i_α} are α-components of coordinate and velocity of the i-th atom, and f_{i_α} is α-component of the force that acts on the i-th atom.

G-K integral converges without any problems in the cases of atomic or simple molecular liquids [10–13]. In liquids with high viscosities, it becomes a challenge to achieve convergence of the G-K integral (5) because of high correlation times of $C_\sigma(t)$. Zhang and Maginn proposed the time decomposition method (TDM) [14] which allows to take G-K integral accurately in the case of ionic liquids and successfully applied it for hydrocarbons [16]. Here, we also use TDM for the viscosity calculation of 2,2,4-trimethylpentane and 2,2,4-trimethylhexane.

For the low pressures (0.1–200 MPa), it is enough to determine $C_\sigma(t)$ up to 100 ps. At higher pressures, $C_\sigma(t)$ is calculated up to 300 ps. The averages for $C_\sigma(t)$ are produced from 30 MD trajectories that are 1 ns long for low pressures and 2 ns long in the cases of high pressures. In the TDM method, the G-K integral is fitted by the double exponential function

$$\eta(t) = A\cdot\alpha\cdot\tau_1\cdot(1-\exp(-t/\tau_1)) + A\cdot(1-\alpha)\cdot\tau_2\cdot(1-\exp(-t/\tau_2)), \quad (8)$$

where A, α, τ_1 and τ_2 are the fitting parameters. Fig. 4a depicts several TDM fits for the different pressures. The $C_\sigma(t)$ long time numerical errors are taken into account with $1/\sigma^{0.5}$ weight in the fitting procedure. We see that the times τ_1 and τ_2 grow with the increase of pressure which can correspond to the more correlated molecular motion at higher pressures. In our recent work, we obtained that these times are connected with the decay times of $C_\sigma(t)$.

The results of the TDM method are shown by arrows on Fig. 4b. We decide to plot them on the dependence of the viscosity on the shear rate as the zero shear rate approximations. It can be seen that the RNEMD points come close to the G-K data with the decrease of shear rate. This fact verifies both techniques converge to the same Newtonian limit and makes us confident that the results are correct. In the following data we use G-K values for the prediction of the shear viscosity of studied hydrocarbons.

4. Viscosity dependence on pressure

4.1. COMPASS verification according to experimental data

The experimental results [34,35] for the viscosity dependence on pressure can be fitted by a function similar to Eq. (2) for density (Fig. 5). Kashiwagi and Makita [71] tried Tait equation as a fit function for the viscosity coefficient but found that the modification of the left part works better for n-dodecane whose viscosity shows strong dependence on pressure:

$$\ln(\eta(P)/\eta_0) = E\cdot\ln[(D+P)/(D+P_0)], \quad (9)$$

where η_0 is a shear viscosity at the pressure P_0, E and D are fitting constants. The usual choice of P_0 is 1 bar = 0.1 MPa. The fitting parameters for the experimental data are shown in Table 2. These experimental data do not show super-Arrhenius behavior in the pressure range observed in the experiments.

The calculated values of η are in good agreement with the experimental values at low pressures up to 100 MPa. The discrepancy grows with the increase of pressure due to overestimated densities from MD (Fig. 2a). The uncertainties for the fitted viscosity values are estimated by the procedure described in Supporting Information. The constants E and D for the fit function and their standard uncertainties are shown in Table 2.

We decide to calculate conventional pressure viscosity coefficient [2] α_0 which is determined as

$$\alpha_0 = \left[\frac{\mathrm{d}(\ln\eta)}{\mathrm{d}P}\right]\Bigg|_{P=0}. \quad (10)$$

It is convenient to use Tait-like fit (9) to find the needed derivative because it already contains $\ln(\eta/\eta_0)$. Thus, $\alpha(P)$ can be found as $E/(D+P)$. The value of $\alpha_0 = E/D$ for 2,2,4-trimethylpentane from the experiment is 10.5±0.4 GPa^{-1}, from the MD calculations α_0 = 10.8±0.6 GPa^{-1}. The simulation results give a very accurate value of the pressure viscosity coefficient.

Taking into account the overestimation at the high pressures, we decided that COMPASS can be used for the prediction of $\eta(P)$ and pressure viscosity coefficient taking into account the density overestimation.

4.2. Prediction for 2,2,4-trimethylhexane

The obtained shear viscosity coefficient $\eta(P)$ dependence on pressure for 2,2,4-trimethylhexane is presented in Fig. 6. The $\eta(P)$ data repeats the trend that is expected from the 2,2,4-trimethylpentane results described above. The data are fitted by Eq. (9) as well. The power E of the exponent is 6.1 which is 1.25 times greater than for 2,2,4-trimethylpentane. It gives faster growth of the viscosity coefficient with the increase of pressure. The pressure viscosity coefficient α_0 is found to be 10.5±0.6 GPa^{-1} which is very close to the 2,2,4-trimethylpentane value. It can be explained by the similarities between the molecules. The benchmark data is also fitted by the Tait-like equation in the pressure range 0.1–500 MPa (black curve on Fig. 6). The benchmark value of α_0 is 9.5±0.6 GPa^{-1}.

The Tait fit of MD data matches the viscosity measurements produced by Scott Bair for the pressures up to 500 MPa within the accuracy of the methods (black open circles on Fig. 6). At the higher pressures, the real pressure viscosity dependence shows super-Arrhenius behavior which is not detected in the current simulation. There are several possible reasons for this discrepancy. First of all, the COMPASS force field may not reproduce the changes in liquid state under these conditions where the super-Arrhenius regime should appear. If COMPASS reproduces the correct state, the problem may lie in a lack of statistics due to the huge relaxation times of SACF at pressures above 500 MPa. The pressure viscosity coefficient α_0 seems to be correct. The predicted density and shear viscosity data at different pressures is shown in Table 3.

Also, we calculated the reciprocal asymptotic isoviscous pressure coefficient α^* which is defined as [2]:

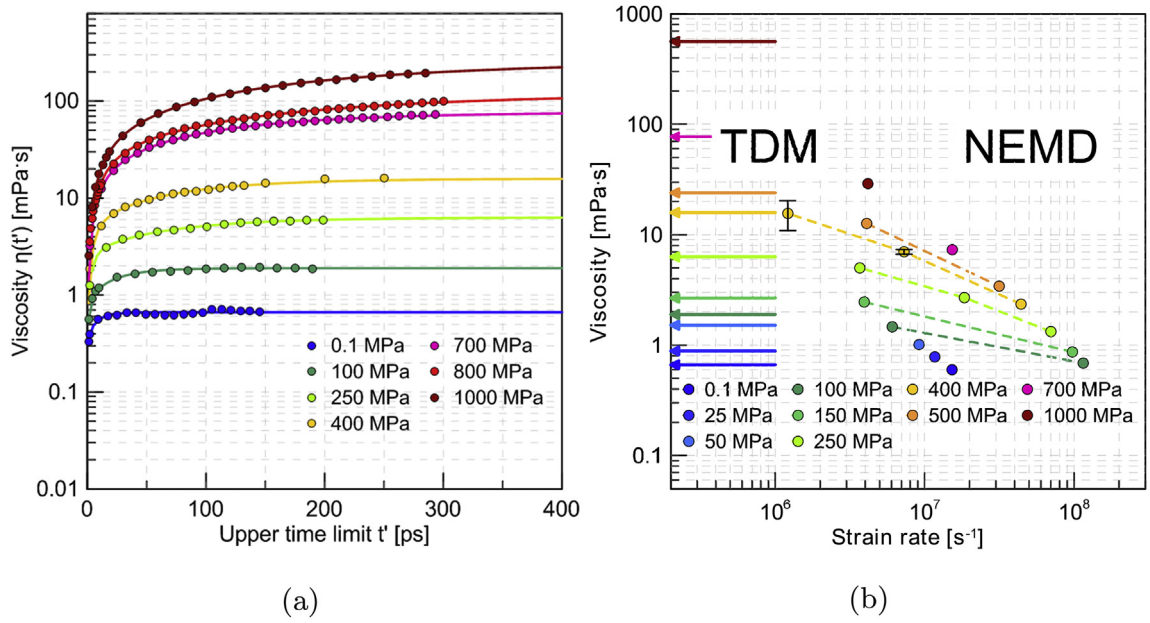

Fig. 4. (a) The dependencies of the Green-Kubo integral on the upper integration limit t' (filled circles) and the double exponential fits obtained using the time decomposition method (8) (solid lines) for 2,2,4-trimethylhexane. (b) The dependence of viscosity on shear rate from NEMD method (filled symbols) and Green-Kubo method (solid lines) as zero shear rate approximation. Same colors denote the same pressures in (a) and (b).

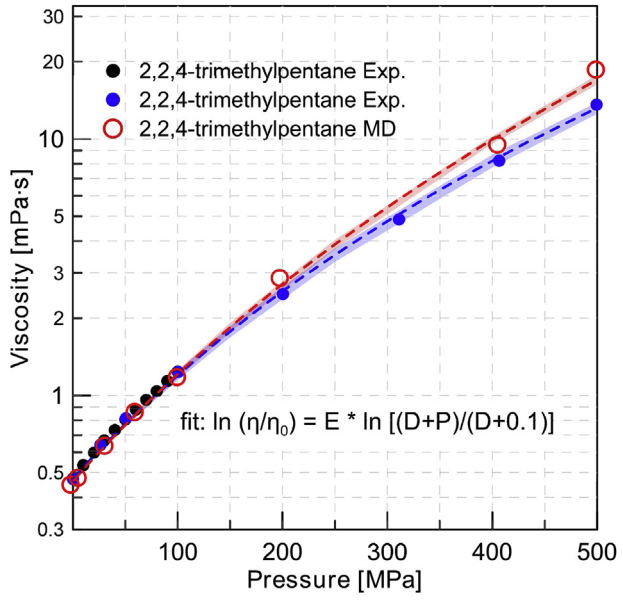

Fig. 5. The shear viscosity dependence on pressure for 2,2,4-trimethylpentane liquid. Red open circles are the simulation results obtained by Green-Kubo, blue and black filled circles are the experimental data [34,35]. The dashed lines are the Tait-like fitting curves from Eq. (9). Red and blue filled areas display the standard deviations for the Tait-like fits.

$$\alpha^* = \left[\int_0^\infty \frac{\eta_0 dp}{\eta(P)}\right]^{-1} \approx \left[\frac{\eta_0}{\alpha_N \eta_N} + \sum_{i=1}^{N} \frac{\eta_0}{\alpha_i} \frac{\eta_i - \eta_{i-1}}{\eta_i \eta_{i-1}}\right], \tag{11}$$

where $\alpha_i = \ln(\eta_i/\eta_{i-1})/(P_i - P_{i-1})$. The obtained value is 8.73 GPa^{-1} which is close to the experimental value of 8.85 GPa^{-1} presented by Scott Bair.

Table 2
The fit parameters E and D for Eq. (9) and errors of the mean for the experimental and simulation data for 2,2,4-trimethylpentane and 2,2,4-trimethylhexane. The last column contains values of pressure viscosity coefficient α_0.

Compound	Method	E	D [MPa]	α_0 [GPa^{-1}]
2,2,4-trimethylpentane	Exp.	3.87 ± 0.35	367 ± 46	10.5 ± 0.4
	MD	4.92 ± 0.76	457 ± 94	10.8 ± 0.6
2,2,4-trimethylhexane	Exp.	8.8 ± 1.5	930 ± 190	9.5 ± 0.6
	MD	6.11 ± 0.77	583 ± 106	10.5 ± 0.6

5. Conclusions

The molecular dynamics calculations of pressure-dependent shear viscosity coefficient and pressure viscosity coefficient are carried out for 2,2,4-trimethylpentane and 2,2,4-trimethylhexane liquids at 293 K. Two computational methods for the shear viscosity are used: reverse non-equilibrium molecular dynamics method (RNEMD) by Müller-Plathe and Green-Kubo integration. The simulations are performed in LAMMPS package using the COMPASS class II force field.

- The RNEMD method can be used for accurate viscosity predictions at low pressures up to 100 MPa. At higher pressures, RNEMD does not allow to obtain the Newtonian viscosity due to the strong dependence of viscosity on shear rate under those conditions. The shear rates created by RNEMD are too high to probe the Newtonian regime. Special techniques must be used for the extrapolation of viscosity values to the zero shear rate. The need to calculate viscosities at multiple shear rates and extrapolate to zero at high pressures brings the computational cost of RNEMD method towards the Green-Kubo method. Therefore, we apply the Green-Kubo method for the viscosity calculations to obtain viscosity at zero shear rate.
- The Green-Kubo (G-K) method has problems with the convergence of the integral of stress autocorrelation functions (SACF) in the highly viscous systems. We use the time-decomposition method developed by Zhang and Maginn in 2015 to estimate

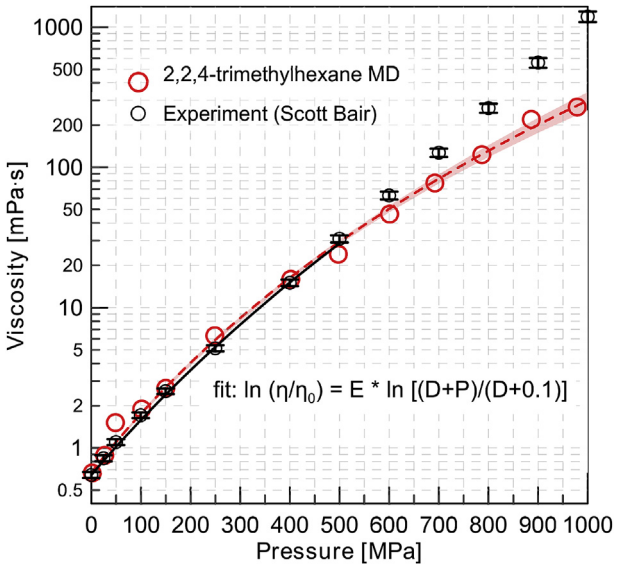

Fig. 6. The shear viscosity dependence on pressure for 2,2,4-trimethylhexane liquid. Red open circles are the simulation results obtained by Green-Kubo integration. The dashed line is Tait-like fit from Eq. (9). Red-filled area displays the standard deviation for the fit. Black open circles are the experimental data obtained by Scott Bair [72]. Black curve is the Tait-like fit of the experimental data from 0.1 to 500 MPa.

Table 3
The computation results for 2,2,4-trimethylhexane liquid at 293 K. The densities ρ are obtained from the NPT simulations. The shear viscosities η are the result of Tait-like fit (9).

P [MPa]	ρ [g/cm^3]	η [mPa·s]	P [MPa]	ρ [g/cm^3]	η [mPa·s]
0.1	0.721	0.663	500	0.890	29.1 ± 1.5
25	0.741	0.856 ± 0.012	600	0.906	49.9 ± 2.3
50	0.757	1.09 ± 0.03	700	0.920	82 ± 4
100	0.784	1.74 ± 0.07	800	0.933	130 ± 7
150	0.804	2.68 ± 0.14	900	0.945	199 ± 14
250	0.836	5.86 ± 0.37	1000	0.955	296 ± 26
400	0.871	16.1 ± 1.0			

the value of the G-K integrals. The low-pressure viscosities obtained from RNEMD and G-K methods agree with each other. For example, at 25 MPa RNEMD gives 0.78 mPa·s (at the shear rate about 10^7 s^{-1}) and G-K gives 0.88 mPa·s. As the pressure grows, the correlation times of SACF become longer which can be a result of more correlated molecular motion. The uncertainty of the computations also grows at the high pressures because one needs to resolve SACF at the long times. The G-K results lie above the RNEMD results because the studied hydrocarbons are shear thinning liquids. We claim that the RNEMD extrapolations to the zero shear rate at each pressure should reach the G-K values.

- The simulation technique is verified by the experimental data for 2,2,4-trimethylpentane at 298 K and pressure range from 0.1 MPa up to 500 MPa. COMPASS overestimates the 2,2,4-trimethylpentane density by 1.5–2% near 500 MPa which leads to the larger values of viscosity. At the low pressures, MD results lie close to the experimental data. The viscosity dependence on pressure can be accurately fitted by a Tait-like equation. The MD and experimental fits overlap within the accuracies of the fitting procedures. The pressure viscosity coefficient is obtained by finding the derivative of the Tait fit. The calculated coefficient 10.8±0.6 GPa^{-1} is close to the experimental value 10.5±0.4 GPa^{-1}.
- The 2,2,4-trimethylhexane density dependence on pressure at 293 K follows the Tait-like equation. It means that the force field reproduces the compressibility of liquid at high pressures. The values of density can be overestimated in comparison with experimental data like in the 2,2,4-trimethylpentane case. The viscosity dependence on pressure is fitted by Tait-like equation for viscosity. The Tait fit of MD data matches the experiment produced by Scott Bair for the pressures up to 500 MPa within the accuracy of the methods. At the higher pressures, the benchmark pressure viscosity dependence shows super-Arrhenius behavior which is not detected in the current simulation. The pressure viscosity coefficient α_0 values are almost the same as for 2,2,4-trimethylpentane which can be explained by the similarities between the molecules. The calculated reciprocal asymptotic isoviscous pressure coefficient α^* value is 8.73 GPa^{-1} and almost matches the experimental value of 8.85 GPa^{-1}. All the data are presented in Table 3.

Acknowledgements

The JIHT part of work is supported by the Russian Science Foundation grant No. 14-50-00124. The work included the development of the MD model and equilibrium MD calculations. The work included non-equilibrium simulations for the verification of equilibrium results has been prepared within the framework of the HSE University Basic Research Program and funded by the Russian Academic Excellence Project 5-100. The calculations are performed on the Desmos and Fisher supercomputers of Joint Institute for High Temperatures RAS.

Authors are very grateful to Genri Norman and Vladimir Stegailov for the stimulating discussions and support. Authors acknowledge LAMMPS developer team, in particular Axel Kohlmeyer, Richard Berger and Trung Nguyen for the prompt fixes of the LAMMPS OpenCL implementation. Also, authors acknowledge Tyler Josephson who drew our attention to this problem.

Appendix A. Supplementary data

Supplementary data to this article can be found online at https://doi.org/10.1016/j.fluid.2019.06.023.

References

[1] D. Dowson, G.R. Higginson, Elasto-hydrodynamic Lubrication: the Fundamentals of Roller and Gear Lubrication, Pergamon Press, 1966.
[2] S. Bair, Y. Liu, Q.J. Wang, The pressure-viscosity coefficient for Newtonian EHL film thickness with general piezoviscous response, J. Tribol. 128 (3) (2006) 624, https://doi.org/10.1115/1.2197846. http://tribology.asmedigitalcollection.asme.org/article.aspx?articleid=1467588.
[3] S. Bair, L. Martinie, P. Vergne, Classical EHL versus quantitative EHL: a perspective Part IISuper-arrhenius piezoviscosity, an essential component of elastohydrodynamic friction missing from classical EHL, Tribol. Lett. 63 (3) (2016) 1–10, https://doi.org/10.1007/s11249-016-0725-4.
[4] E.J. Maginn, J.R. Elliott, Historical perspective and current outlook for molecular dynamics as a chemical engineering tool, Ind. Eng. Chem. Res. 49 (7) (2010) 3059–3078, https://doi.org/10.1021/ie901898k. http://pubs.acs.org/doi/abs/10.1021/ie901898k.
[5] J.P. Ewen, D.M. Heyes, D. Dini, Advances in nonequilibrium molecular dynamics simulations of lubricants and additives, Friction (Md) 6 (4) (2018) 349–386, https://doi.org/10.1007/s40544-018-0207-9. http://link.springer.com/10.1007/s40544-018-0207-9.
[6] E. Helfand, Transport coefficients from dissipation in a canonical ensemble, Phys. Rev. 119 (1) (1960) 1–9.
[7] A.W. Lees, S.F. Edwards, The computer study of transport processes under extreme conditions, J. Phys. Condens. Matter 5 (15) (1972) 1921.
[8] D.J. Evans, G.P. Morriss, Nonlinear-response theory for steady planar Couette flow, Phys. Rev. A 30 (3) (1984) 1528.
[9] F. Müller-Plathe, Reversing the perturbation in nonequilibrium molecular dynamics: an easy way to calculate the shear viscosity of fluids, Phys. Rev. E 59 (5) (1999) 4894–4898.
[10] D. Nevins, F.J. Spera, Accurate computation of shear viscosity from equilibrium molecular dynamics simulations, Mol. Simul. 33 (15) (2007) 1261–1266, https://doi.org/10.1080/08927020701675622. http://www.tandfonline.com/doi/abs/10.1080/08927020701675622.

[11] V.Y. Rudyak, S.L. Krasnolutskii, Dependence of the viscosity of nanofluids on nanoparticle size and material, Phys. Lett. A. 378 (26–27) (2014) 1845–1849, https://doi.org/10.1016/j.physleta.2014.04.060. https://doi.org/10.1016/j.physleta.2014.04.060.
[12] V.Y. Rudyak, S. Krasnolutskii, Simulation of the nanofluid viscosity coefficient by the molecular dynamics method, Tech. Phys. 60 (6) (2015) 798–804. https://doi.org/10.1134/S1063784215060237.
[13] M. Chen, J.R. Vella, A.Z. Panagiotopoulos, P.G. Debenedetti, F.H. Stillinger, E.A. Carter, Liquid li structure and dynamics: a comparison between OFDFT and second nearest-neighbor embedded-atom method, AIChE J. 61 (9) (2015) 2841–2853, https://doi.org/10.1002/aic.14795, 0201037v1, http://doi.wiley.com/10.1002/aic.14795.
[14] Y. Zhang, A. Otani, E.J. Maginn, Reliable viscosity calculation from equilibrium molecular dynamics simulations: a time decomposition method, J. Chem. Theory Comput. 11 (8) (2015) 3537–3546, https://doi.org/10.1021/acs.jctc.5b00351. http://pubs.acs.org/doi/abs/10.1021/acs.jctc.5b00351.
[15] Y. Zhang, L. Xue, F. Khabaz, R. Doerfler, E.L. Quitevis, R. Khare, E.J. Maginn, Molecular topology and local dynamics govern the viscosity of imidazolium-based ionic liquids, J. Phys. Chem. B 119 (47) (2015) 14934–14944, https://doi.org/10.1021/acs.jpcb.5b08245. http://pubs.acs.org/doi/10.1021/acs.jpcb.5b08245.
[16] O.A. Moultos, Y. Zhang, I.N. Tsimpanogiannis, I.G. Economou, E.J. Maginn, System-size corrections for self-diffusion coefficients calculated from molecular dynamics simulations: the case of CO2, n -alkanes, and poly(ethylene glycol) dimethyl ethers, J. Chem. Phys. 145 (7) (2016), 074109, https://doi.org/10.1063/1.4960776. https://doi.org/10.1063/1.4960776.
[17] K.S. Kim, M.H. Han, C. Kim, Z. Li, G.E. Karniadakis, E.K. Lee, Nature of intrinsic uncertainties in equilibrium molecular dynamics estimation of shear viscosity for simple and complex fluids, J. Chem. Phys. 149 (4) (2018), 044510, https://doi.org/10.1063/1.5035119 arXiv:1807.08063.
[18] B. Hess, Determining the shear viscosity of model liquids from molecular dynamics simulations, J. Chem. Phys. 116 (1) (2002) 209–217, https://doi.org/10.1063/1.1421362.
[19] J.P. Ewen, C. Gattinoni, F.M. Thakkar, N. Morgan, H.A. Spikes, D. Dini, A comparison of classical force-fields for molecular dynamics simulations of lubricants, Materials 9 (8) (2016) 1–17, https://doi.org/10.3390/ma9080651, 1706.00179.
[20] D.J. Evans, P.T. Cummings, Nonequilibrium molecular dynamics properties and non Newtonian fluid approaches to transport rheology, Ind. Eng. Chem. Res. 31 (1992) 1237–1252, https://doi.org/10.1021/ie00005a001.
[21] J.D. Moore, S.T. Cui, H.D. Cochran, P.T. Cummings, Rheology of lubricant basestocks: a molecular dynamics study of C_{30} isomers, J. Chem. Phys. 113 (19) (2000) 8833, https://doi.org/10.1063/1.1318768. http://scitation.aip.org/content/aip/journal/jcp/113/19/10.1063/1.1318768.
[22] L.I. Kioupis, E.J. Maginn, Impact of molecular architecture on the high-pressure rheology of hydrocarbon fluids, J. Phys. Chem. B 104 (32) (2000) 7774–7783, https://doi.org/10.1021/jp000966x. https://pubs.acs.org/doi/10.1021/jp000966x.
[23] C. McCabe, S. Cui, P.T. Cummings, Characterizing the viscositytemperature dependence of lubricants by molecular simulation, Fluid Phase Equilib. 183–184 (2001) 363–370, https://doi.org/10.1016/S0378-3812(01)00448-4. https://linkinghub.elsevier.com/retrieve/pii/S0378381201004484.
[24] C. McCabe, S. Cui, P.T. Cummings, P.A. Gordon, R.B. Saeger, Examining the rheology of 9-octylheptadecane to giga-pascal pressures, J. Chem. Phys. 114 (4) (2001) 1887–1891, https://doi.org/10.1063/1.1334676. http://aip.scitation.org/doi/10.1063/1.1334676.
[25] S. Bair, C. McCabe, P.T. Cummings, Comparison of nonequilibrium molecular dynamics with experimental measurements in the nonlinear shear-thinning regime, Phys. Rev. Lett. 88 (5) (2002), 058302, https://doi.org/10.1103/PhysRevLett.88.058302. https://link.aps.org/doi/10.1103/PhysRevLett.88.058302.
[26] C. McCabe, C.W. Manke, P.T. Cummings, Predicting the Newtonian viscosity of complex fluids from high strain rate molecular simulations, J. Chem. Phys. 116 (8) (2002) 3339–3342, https://doi.org/10.1063/1.1446045. http://aip.scitation.org/doi/10.1063/1.1446045.
[27] G. Pan, C. McCabe, Prediction of viscosity for molecular fluids at experimentally accessible shear rates using the transient time correlation function formalism, J. Chem. Phys. 125 (19) (2006) 194527, https://doi.org/10.1063/1.2364899. http://aip.scitation.org/doi/10.1063/1.2364899.
[28] V. Jadhao, M.O. Robbins, Probing large viscosities in glass-formers with nonequilibrium simulations, Proc. Natl. Acad. Sci. U.S.A. (2017) 201705978, https://doi.org/10.1073/pnas.1705978114. http://www.pnas.org/lookup/doi/10.1073/pnas.1705978114.
[29] W. Allen, R.L. Rowley, Predicting the viscosity of alkanes using nonequilibrium molecular dynamics: evaluation of intermolecular potential models, J. Chem. Phys. 106 (24) (1997) 10273, https://doi.org/10.1063/1.474052. http://scitation.aip.org/content/aip/journal/jcp/106/24/10.1063/1.474052.
[30] W.L. Jorgensen, D.S. Maxwell, J. Tirado-Rives, Development and testing of the OPLS all-atom force field on conformational energetics and properties of organic liquids, J. Am. Chem. Soc. 118 (45) (1996) 11225–11236. http://pubs.acs.org/doi/abs/10.1021/ja9621760.
[31] W.L. Jorgensen, J.D. Madura, C.J. Swenson, Optimized intermolecular potential functions for liquid hydrocarbons, J. Am. Chem. Soc. 106 (22) (1984) 6638–6646.
[32] M. Lahtela, M. Linnolahti, T.A. Pakkanen, R.L. Rowley, Computer simulations of branched alkanes: the effect of side chain and its position on rheological behavior, J. Chem. Phys. 108 (6) (1998) 2626–2630, https://doi.org/10.1063/1.475649.
[33] M.J. Comuñas, X. Paredes, F.M. Gaciño, J. Fernández, J.-P. Bazile, C. Boned, J.-L. Daridon, G. Galliero, J. Pauly, K.R. Harris, Viscosity measurements for squalane at high pressures to 350MPa from T=(293.15 to 363.15)K, J. Chem. Thermodyn. 69 (2014) 201–208, https://doi.org/10.1016/j.jct.2013.10.001. http://linkinghub.elsevier.com/retrieve/pii/S0021961413003686.
[34] J.H. Dymond, N.F. Glen, J.D. Isdale, Transport properties of nonelectrolyte liquid mixtures-VII. Viscosity coefficients for isooctane and for equimolar mixtures of isooctane + n-octane and isooctane + n-dodecane from 25 to 100 C at pressures up to 500 MPa or to the freezing pressure, Int. J. Thermophys. 6 (3) (1985) 233–250, https://doi.org/10.1007/BF00522146.
[35] A.A. Pádua, J.M. Fareleira, J.C. Calado, W.A. Wakeham, Density and viscosity measurements of 2,2,4-trimethylpentane (isooctane) from 198 K to 348 K and up to 100 MPa, J. Chem. Eng. Data 41 (6) (1996) 1488–1494, https://doi.org/10.1021/je950191z.
[36] J.H. Dymond, R. Malhotra, The Tait equation: 100 years on, Int. J. Thermophys. 9 (6) (1988) 941–951, https://doi.org/10.1007/BF01133262.
[37] Y.D. Fomin, V.V. Brazhkin, V.N. Ryzhov, Isoviscosity lines and the liquid-glass transition in simple liquids, Phys. Rev. E 86 (1) (2012) 1–5, https://doi.org/10.1103/PhysRevE.86.011503.
[38] R.E. Ryltsev, N.M. Chtchelkatchev, Multistage structural evolution in simple monatomic supercritical fluids: superstable tetrahedral local order, Phys. Rev. E 88 (5) (2013), 052101, https://doi.org/10.1103/PhysRevE.88.052101. http://link.aps.org/doi/10.1103/PhysRevE.88.052101.
[39] R.E. Ryltsev, N.M. Chtchelkatchev, Hydrodynamic anomalies in supercritical fluid, J. Chem. Phys. 141 (12) (2014) 124509, https://doi.org/10.1063/1.4895726, 1407.5462.
[40] M.A. Orekhov, Fluctuation enhancement of ion diffusivity in liquids, Phys. Chem. Chem. Phys. 19 (2017) 32398–32403, https://doi.org/10.1039/C7CP07170A. https://doi.org/10.1039/C7CP07170A.
[41] H. Hu, L. Bao, N.V. Priezjev, K. Luo, Identifying two regimes of slip of simple fluids over smooth surfaces with weak and strong wall-fluid interaction energies, J. Chem. Phys. 146 (3) (2017), 034701, https://doi.org/10.1063/1.4973640. https://doi.org/10.1063/1.4973640. https://doi.org/10.1063/1.4973640.
[42] S. Shahruddin, G. Jiménez-Serratos, G.J.P. Britovsek, O.K. Matar, E.A. Müller, Fluid-solid phase transition of n-alkane mixtures: coarse-grained molecular dynamics simulations and diffusion-ordered spectroscopy nuclear magnetic resonance, Sci. Rep. 9 (1) (2019), https://doi.org/10.1038/s41598-018-37799-7, 1002; 1002–1002, https://www.ncbi.nlm.nih.gov/pubmed/30700804.
[43] M.G. Martin, J.I. Siepmann, Transferable potentials for phase equilibria. 1. United-atom description of n -alkanes, J. Phys. Chem. B 102 (14) (1998) 2569–2577, https://doi.org/10.1021/jp972543+. http://pubs.acs.org/doi/abs/10.1021/jp972543{%}2B.
[44] N.D. Orekhov, V.V. Stegailov, Graphite melting: atomistic kinetics bridges theory and experiment, Carbon N. Y. 87 (C) (2015) 358–364, https://doi.org/10.1016/j.carbon.2015.02.049. https://doi.org/10.1016/j.carbon.2015.02.049.
[45] Y.D. Fomin, V.N. Ryzhov, E.N. Tsiok, The behavior of cyclohexane confined in slit carbon nanopore, J. Chem. Phys. 143 (18) (2015) 184702, https://doi.org/10.1063/1.4935197. http://scitation.aip.org/content/aip/journal/jcp/143/18/10.1063/1.4935197.
[46] E. Iakovlev, P. Zhilyaev, I. Akhatov, Atomistic study of the solid state inside graphene nanobubbles, Sci. Rep. 7 (1) (2017) 17906.
[47] A. Korotkevich, D.S. Firaha, A.A. Padua, B. Kirchner, Ab Initio Molecular Dynamics Simulations of So2 Solvation in Choline Chloride/glycerol Deep Eutectic Solvent, vol. 448, Fluid Ph. Equilibria, 2017, pp. 59–68, deep Eutectic Solvents, https://doi.org/10.1016/j.fluid.2017.03.024, http://www.sciencedirect.com/science/article/pii/S0378381217301267.
[48] I. Androniuk, C. Landesman, P. Henocq, A.G. Kalinichev, Adsorption of gluconate and uranyl on c-s-h phases: combination of wet chemistry experiments and molecular dynamics simulations for the binary systems, Phys. Chem. Earth (2017) 194–203. P. A/B/C 99, https://doi.org/10.1016/j.pce.2017.05.005, http://www.sciencedirect.com/science/article/pii/S1474706516302601. mechanisms and Modelling of Waste-Cement and Cement-Host Rock Interactions.
[49] D.V. Minakov, M.A. Paramonov, P.R. Levashov, Consistent interpretation of experimental data for expanded liquid tungsten near the liquid-gas coexistence curve, Phys. Rev. B 97 (2018), 024205, https://doi.org/10.1103/PhysRevB.97.024205. https://link.aps.org/doi/10.1103/PhysRevB.97.024205.
[50] E.M. Kirova, G.E. Norman, V.V. Pisarev, Viscosity of aluminum during the glass transition process, according to molecular dynamics, Russ. J. Phys. Chem. A 92 (10) (2018) 1865–1869, https://doi.org/10.1134/S0036024418100126. https://doi.org/10.1134/S0036024418100126.
[51] V. Pisarev, S. Mistry, Volume-based mixing rules for viscosities of methane + n-butane liquid mixtures, Fluid Phase Equilib. 484 (2019) 98–105. https://doi.org/10.1016/j.fluid.2018.11.020. http://www.sciencedirect.com/science/article/pii/S0378381218304795.
[52] G. Ostroumova, N. Orekhov, V. Stegailov, Reactive molecular-dynamics study of onion-like carbon nanoparticle formation, Diam. Relat. Mater. 94 (2019) 14–20. https://doi.org/10.1016/j.diamond.2019.01.019. http://www.sciencedirect.com/science/article/pii/S0925963518306915.
[53] N.D. Kondratyuk, G.E. Norman, V.V. Stegailov, Self-consistent molecular dynamics calculation of diffusion in higher n-alkanes, J. Chem. Phys. 145 (20) (2016) 204504.

[54] K.A. Maerzke, J.I. Siepmann, Transferable potentials for phase equilibria - coarse-Grain description for linear alkanes, J. Phys. Chem. B 115 (13) (2011) 3452–3465, https://doi.org/10.1021/jp1063935.
[55] T. C. O'Connor, J. Andzelm, M. O. Robbins, AIREBO-M: a reactive model for hydrocarbons at extreme pressures, J. Chem. Phys. 142 (2). 024903, arXiv: NIHMS150003, doi:10.1063/1.4905549. URL https://doi.org/10.1063/1.4905549.
[56] H. Sun, COMPASS: an ab initio force-field optimized for condensed-phase Applications s overview with details on alkane and benzene compounds, J. Phys. Chem. 5647 (98) (1998) 7338–7364, https://doi.org/10.1021/jp980939v.
[57] Compass Parameters at the Lammps Forum, https://lammps.sandia.gov/threads/msg11270.html, accessed: 2018-09-27.
[58] K.-S. Kim, M.H. Han, C. Kim, Z. Li, G.E. Karniadakis, E.K. Lee, Nature of intrinsic uncertainties in equilibrium molecular dynamics estimation of shear viscosity for simple and complex fluids, J. Chem. Phys. 149 (4) (2018), 044510, https://doi.org/10.1063/1.5035119.
[59] I.C. Yeh, G. Hummer, System-size dependence of diffusion coefficients and viscosities from molecular dynamics simulations with periodic boundary conditions, J. Phys. Chem. B 108 (40) (2004) 15873–15879, https://doi.org/10.1021/jp0477147.
[60] N.A. Volkov, M.V. Posysoev, A.K. Shchekin, The effect of simulation cell size on the diffusion coefficient of an ionic surfactant aggregate, Colloid J. 80 (3) (2018) 248–254, https://doi.org/10.1134/S1061933X1803016X. https://doi.org/10.1134/S1061933X1803016X.
[61] R. Hockney, J. Eastwood, Computer Simulation Using Particles, CRC Press, New York, 1989.
[62] M. Tuckerman, B.J. Berne, G.J. Martyna, Reversible multiple time scale molecular dynamics, J. Chem. Phys. 97 (3) (1992) 1990–2001, https://doi.org/10.1063/1.463137. https://doi.org/10.1063/1.463137. https://doi.org/10.1063/1.463137.
[63] S. Plimpton, Fast parallel algorithms for short-range molecular dynamics, J. Comput. Phys. 117 (1) (1995) 1–19, https://doi.org/10.1006/jcph.1995.1039. http://linkinghub.elsevier.com/retrieve/pii/S002199918571039X.
[64] W.M. Brown, P. Wang, S.J. Plimpton, A.N. Tharrington, Implementing molecular dynamics on hybrid high performance computers - short range forces, Comput. Phys. Commun. 182 (2011) 898–911.
[65] W.M. Brown, A. Kohlmeyer, S.J. Plimpton, A.N. Tharrington, Implementing molecular dynamics on hybrid high performance computers - particle-particle particle-mesh, Comput. Phys. Commun. 183 (2012) 449–459.
[66] W.M. Brown, Y. Masako, Implementing molecular dynamics on hybrid high performance computers - three-body potentials, Comput. Phys. Commun. 184 (2013) 2785–2793.
[67] V. Stegailov, A. Agarkov, S. Biryukov, T. Ismagilov, M. Khalilov, N. Kondratyuk, E. Kushtanov, D. Makagon, A. Mukosey, A. Semenov, A. Simonov, A. Timofeev, V. Vecher, Early performance evaluation of the hybrid cluster with torus interconnect aimed at molecular-dynamics simulations, in: R. Wyrzykowski, J. Dongarra, E. Deelman, K. Karczewski (Eds.), Parallel Processing and Applied Mathematics, Springer International Publishing, Cham, 2018, pp. 327–336.
[68] N. Kondratyuk, G. Smirnov, E. Dlinnova, S. Biryukov, V. Stegailov, Hybrid supercomputer desmos with torus angara interconnect: efficiency analysis and optimization, in: L. Sokolinsky, M. Zymbler (Eds.), Parallel Computational Technologies, Springer International Publishing, Cham, 2018, pp. 77–91.
[69] N. Kondratyuk, G. Smirnov, V. Stegailov, Hybrid codes for atomistic simulations on the desmos supercomputer: gpu-acceleration, scalability and parallel i/o, in: V. Voevodin, S. Sobolev (Eds.), Supercomputing, Springer International Publishing, Cham, 2019, pp. 218–229.
[70] V. Stegailov, E. Dlinnova, T. Ismagilov, M. Khalilov, N. Kondratyuk, D. Makagon, A. Semenov, A. Simonov, G. Smirnov, A. Timofeev, Angara interconnect makes gpu-based desmos supercomputer an efficient tool for molecular dynamics calculations, Int. J. High Perform. Comput. Appl. 33 (3) (2019) 507–521. https://doi.org/10.1177/1094342019826667.
[71] H. Kashiwagi, T. Makita, Viscosity of twelve hydrocarbon liquids in the temperature range 298-348 K at pressures up to 110 MPa, Int. J. Thermophys. 3 (4) (1982) 289–305, https://doi.org/10.1007/BF00502346.
[72] Results for the 10th Industrial Fluid Properties Simulation Challenge, Produced by Scott Bair, http://fluidproperties.org/10th-benchmarks, accessed: 2019-02-21.